Dalton Transactions

Accepted Manuscript

ROYAL SOCIETY OF CHEMISTRY

www.rsc.org/dalton

Dalton Transactions

RSCPublishing

ARTICLE

Influence of substituents on cation-anion contacts in imidazolium perrhenates

Cite this: DOI: 10.1039/x0xx00000x

Robert M. Reich,[a,†] Mirza Cokoja,[a,*] Iulius I. E. Markovits,[a,†] Christian J. Münchmeyer,[a,†] Marlene Kaposi,[a] Alexander Pöthig,[a] Wolfgang A. Herrmann[a] and Fritz E. Kühn[a,*]

Received 00th February 2015,
Accepted 00th January 2012

DOI: 10.1039/x0xx00000x

www.rsc.org/dalton

A series of imidazolium perrhenates with different substituents at the imidazolium ring were synthesised and characterised, including single crystal X-ray diffraction. The effect of the substitution pattern on the state of aggregation of the compounds, the charge delocalisation and the ion pairing interaction via hydrogen bonds was studied. Particularly the substitution at the C2 position of the imidazolium ring was shown to be crucial to fine-tune the ion contacts. Fluorinated substituents appear to exhibit enhanced interionic interactions. The ability to tune the degree of contacts of the perrhenate anion allows for adjusting the nucleophilicity of this anion.

Introduction

Ionic compounds containing an organic cation and weakly coordinating anions have received considerable attention in recent years. The possibility to permute different ions and to provide the organic cation with functional groups opens the door to a plethora of tailor-made materials with tuneable properties. The most prominent representatives of this class of compounds are ionic liquids (IL),[1] which have found applications as solvents or reaction media with unique properties, such as high polarity and concomitant hydrophobicity.[2-5] Small variations on the cationic structure results in a significant change of physicochemical behaviour of the ILs.[6-11] Therefore, an understanding of the influence of different substitution patterns on the physicochemical properties is essential to get an insight in the rational design of functional ionic compounds.[12-15]

Various studies focused on the influence of the alkylation of the wing tip groups in imidazolium-based ILs[12,16-21] and on methylation of the C2 position at the imidazolium cation.[12, 22-25] Additionally, Strassner et al. showed that different substitution patterns on the imidazolium moiety lead to a significant change of the electron density distribution on the cation and therefore provide insight on the interaction sites between anion and cation.[26,27] Theoretical studies by Ludwig et al. show that the C2 position of the imidazolium cation possesses a strong positive partial charge, which can be reduced by methylation of the C2 position.[22] Therefore, changing the substitution pattern on this position has a strong influence not only on the distance between cation and anion, but also on the electronic structure of the entire compound. These effects are particularly well studied for imidazolium-based ionic compounds.[28] Studies performed by the groups of Ludwig[22] and Hunt[23,24] show that the interaction strength between anion and cation can be controlled by the substitution of the hydrogen atom on the C2 position. The methylation of the C2 position leads to an equal distribution of the positive charge on the imidazolium ring, thus weakening the strong partial positive charge that acts as dominant binding site to the anion.

Recently we have reported the epoxidation of olefins with hydrogen peroxide as oxidant using imidazolium perrhenate ($[ReO_4]^-$) ILs as promoters, showing that the cation has a major impact on the reactivity of these ILs.[29] The principle of the activity of the perrhenate anion is based on weak ion interactions allowing for activation of H_2O_2 by hydrogen bonding to $[ReO_4]^-$ and subsequent oxygen transfer to an olefin. Consequently, when cations such as K^+ and $[NH_4]^+$ are used, which are able to form strong interactions to the anion, the activity of the perrhenate ion is significantly lower. Principally, in imidazolium perrhenates the cation-anion interactions primarily involve H–O contacts, where the proton is located at the C2 position of the imidazolium ring. Accordingly, substitution of the proton at the C2 position by alkyl groups should delocalise the positive charge over the cation and decrease the ion pairing, rendering the anion less sterically encumbered and thus more nucleophilic. This would be beneficial for the epoxidation reaction. For this work, a series of imidazolium perrhenates was synthesised and the influence of the substitution of different alkyl groups at the C2 ring position was studied. Additionally, the influence of the wing tip groups at the nitrogen atoms was examined via single crystal X-ray analysis combined with Hirshfeld surface analysis and by DFT calculations on the distribution of charge density.

Results and Discussion

Synthesis and characterisation

All imidazolium perrhenates were synthesised according to a recently published procedure.[29] As shown in Scheme 1, the substituents at the nitrogen atoms and at the C2 position were varied. Benzyl (Bn) and 2',3',4',5',6'-pentafluorobenzyl (Bn^F) wing tips were chosen as they usually lead to imidazolium compounds exhibiting melting points well above room temperature (see the Experimental Section for details) and could therefore be crystallised.

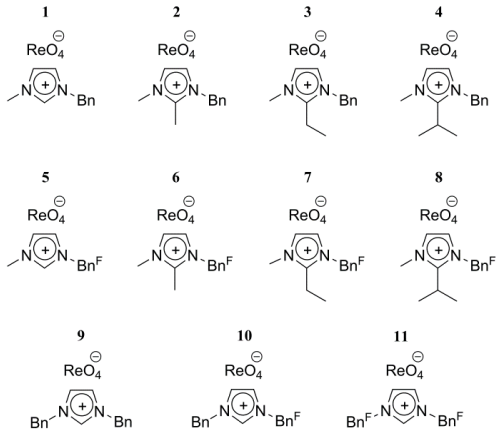

Scheme 1. Overview of the synthesised ionic compounds (Bn = benzyl, Bn^F = 2',3',4',5',6'-pentafluorobenzyl)).

It is noteworthy that the substitution pattern significantly influences the melting points (Figure 1). It is known that these changes are indicators for higher interionic interactions.[22-24] Studies of Ludwig et al. show that methylation of an imidazolium cation leads to a decrease of long range van-der-Waals interactions, which therefore should affect the anion-cation interaction.[22] However, an increase of the Coulomb interaction enhances the interionic interactions. These interionic interactions lead, on a macroscopic level, to the observed melting points.[12] Since the melting points also depend on the packing of the ions, which correlates to their symmetry, cations with high symmetry have higher melting points.[30,31] This behaviour is observed for compounds **2**, **3** and **4**, where the symmetry increases from Et < ^{i}Pr < Me.

Fluorination leads to a distinct increase in melting points compared to the alkylated compounds (*c.f.* compounds **5**–**8** and **1**–**4**). It implies that fluorination also enhances the Coulomb interactions, leading to stronger anion-cation contacts. The dibenzyl compounds **9**–**11** confirm the tendency that a fluorination as such increases the melting points and therefore the interionic interactions. The similar melting points of the half-fluorinated compound **10** with the highly symmetric dibenzyl compound **9** underlines this fact as it is known that high symmetry leads to increased melting points. Therefore the fully fluorinated and highly symmetric compound **11** exhibits a very high melting point. Hence, these observations have prompted us to examine the X-ray single crystal structures of compounds **1**–**11** in more detail in order to elucidate, in which way the nature and strength of the ion contacts is influenced by substitution of the C2 proton. To gain more and quantifiable insights in the cation-anion interactions spectroscopic methods, DFT calculations and Hirshfeld surface analysis were additionally applied.

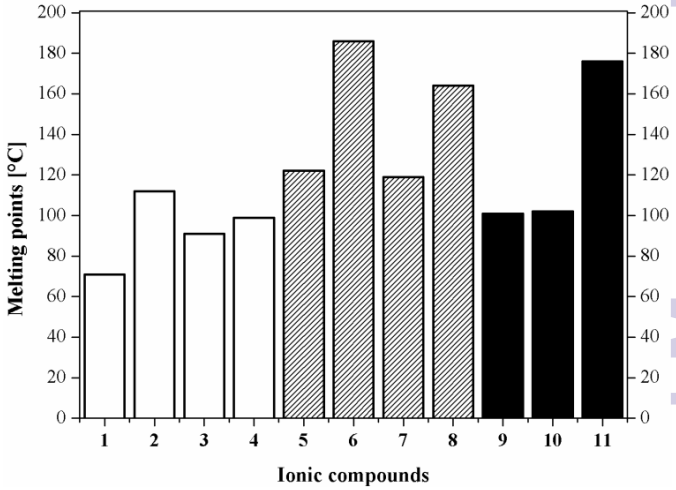

Figure 1. Illustration of melting points of compounds **1–11**.

Spectroscopic Studies

^{1}H- and ^{13}C-NMR spectra of compounds **1**–**8** indicate a changed electron density upon alkylation on the C2 position. As it is known that upfield resonance shifts are an indicator for a higher electron density,[12] the upfield shifts of the backbone protons after alkylation suggest a change in the O–H contact between the cation and $[ReO_4]^-$, which appears to donate more electron density to the backbone protons (Table 1). The simultaneous downfield shift of the C2 carbon (Table 1) was also observed by Wasserscheid et al. by the examination of the C2 position in different NTf_2-based ionic liquids.[12] It was argued that the ability of the anion to push electron density to the C2 carbon decreased upon methylation due to the rearrangement of the anion in solution. In the cases described here, NMR studies corroborate these findings, showing that alkylation leads to a possible reorientation of the anion and cation. As result, the anion is located closer towards the backbone protons.

Table 1. ^{1}H- and ^{13}C-NMR studies of compounds **1**–**8**.[a]

Entry	Compounds	^{1}H-NMR [ppm] Backbone-H	^{13}C-NMR [ppm] C2 position C
1	**1**	7.78/7.71	136.7
2	**2**	7.70/7.65	144.6
3	**3**	7.72/7.69	148.0
4	**4**	7.71/7.69	149.3
5	**5**	7.77/7.73	137.7
6	**6**	7.66/7.63	145.2
7	**7**	7.69/7.62	148.4
8	**8**	7.68/7.58	149.6

[a] NMR sample preparation: 50.0 mg of sample and 0.4 ml of DMSO-d_6 were used.

DFT studies

DFT calculations of the imidazolium cation corroborate the reorientation of anion and cation shown by NMR spectroscopy caused by alkylation of the C2 position of the imidazolium ring. The main positive charge of the imidazolium cation of compound **1** is clearly located between the nitrogen atoms (Figure 2, far left). Methylation reduces the strong positive partial charge and leads to an increased charge delocalisation (Figure 2, middle left).

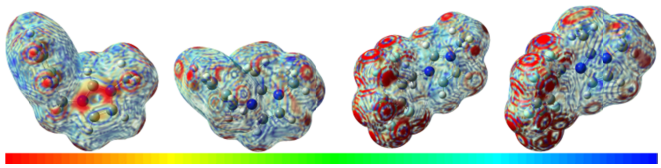

Figure 2. Distribution of charge densities for the cations $[MeBnIm]^+$ (**1**, far left, Me = methyl, Bn = benzyl, Im = imidazolium) and $[MeMeBnIm]^+$ (**2**, middle left), $[MeBn^FIm]^+$ (**5**, middle right) and $[MeMeBn^FIm]^+$ (**6**, far right) in the gas phase (B3LYP/6-311++G(d,p) level of theory). The range of the scale lasts from $3.770e^{-4}$ (red, less electron density) to $3.990e^{-4}$ (blue, more electron density). The numbers represent energy per charge in units of Hartree per elemental charge.

This should result in reduced ion contact strengths, which is in accord with the observed downfield shift of the backbone protons in ^{1}H-NMR from compound **2** to **1** as the anion donates less electron density to the backbone protons in compound **1** as its main interaction site is the protonated C2-position. This assumption is also supported by the upfield shift of the C2 carbon resonance in the ^{13}C-NMR, which is in agreement with previous observations of Wasserscheid et al.[12] The dominating influence of the Bn^F groups is also seen in the distribution of the charge density in the cation $[MeBn^FIm]^+$ (Figure 2, middle right). The electron density is concentrated on the imidazolium cation. Less electron density is found on the Bn^F moiety, implying that a contact of the Bn^F group and $[ReO_4]^-$ should be possible. Furthermore, the electron density of the methylated cation $[MeMeBn^FIm]^+$ (Figure 2, far right) shows that a change of the C2 substituent does not lead to a significant change in the electron density of the imidazolium cation compared to the non-fluorinated cations of compounds **1** and **2**.

Further DFT calculations of the dibenzylated cation of **9** and the 1,3-dibenzyl-2-methylimidazolium cation **10** were also performed (Figure 3). In comparison to the monobenzyl-substituted cations of compounds **1** and **2** the distribution of the charge density is similar for compounds **2** and **10**.

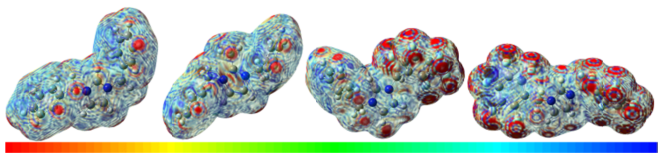

Figure 3. Distribution of charge densities for $[BnBnIm]^+$ (cation of compound **9**, far left), $[BnMeBnIm]^+$ (middle left), $[BnBn^FIm]^+$ (**10**, middle right) and $[Bn^FBn^FIm]^+$ (**11**, far right) in the gas phase (B3LYP/6-311++G(d,p) level of theory). The range of the scale lasts from $3.770e^{-4}$ (red, less electron density) to $3.990e^{-4}$ (blue, more electron density). The numbers represent energy per charge in units of Hartree per elemental charge.

Apparently, for C2 methylated imidazolium cations, a symmetric or asymmetric substitution at the nitrogen atoms has a minor effect on the cation-anion interaction. Therefore, the steric repulsion of two Bn groups seems to be more relevant. Fluorination in the compounds **10** to **11** show that less electron density is found on the Bn^F moiety, as also seen for the compounds **5**–**8** compared to **1**–**4**. Similarly to the charge distribution in the cations of compounds **5** and **6**, interaction of the $[ReO_4]^-$ anion with the Bn^F wing tips in **10** and **11** is possible.

X-Ray single crystal structure analysis

The molecular structures of compounds **1**–**11** can give a more detailed insight in the anion-cation interaction and the nature of these interactions in the solid state. The main interaction is a contact of one of the oxygen atoms of $[ReO_4]^-$ with the acidic proton at the C2 position of the imidazolium cation. It is well known that this proton is able to interact with the anion (e.g. bromide and NTf_2 salts).[12] This contact can even lead to an abstraction of the proton to form a stable *N*-heterocyclic carbene, as it was reported by Rogers et al. with acetate-containing imidazolium-based ionic liquids.[32] Therefore, the main focus lies on the interaction of the oxygen atoms of the perrhenate anion (donor) with the acidic protons (and its corresponding carbon atoms as acceptor) of the imidazolium cation.

The Hirshfeld surface analysis provides the possibility to quantify the strength and nature of interactions between cations and anions in a crystal with the help of a calculated contracted hydrogen atom electron density.[33] Therefore, it is a valuable method to analyse the type and quantity of the electron donor ($[ReO_4]^-$) and electron acceptor (imidazolium cation) interaction. As shown by X-ray single crystal structure analysis, the perrhenate anion of **1** is located at the C2 position of the imidazolium cation, since this is the most acidic position (Figure 4). DFT calculations show that the main positive charge of the imidazolium cation is located between the nitrogen atoms (Figure 2, far left). This high partial charge results in a strong interaction between cation and anion, represented by the shortest OH contact of 2.249 Å (or OC 3.027(4) Å, respectively; see Table 2, Entry 1).

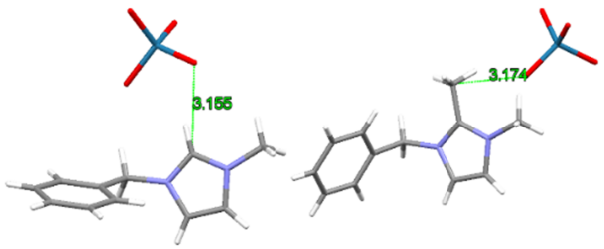

Figure 4. View of the molecular structures of $[MeBnIm][ReO_4]$ (**1**, left) and **2** $[MeMeBnIm][ReO_4]$ (**2**, right) with the shortest interatomic OC distance (H = white, N = blue, C = grey, Re = turquois, O = red).

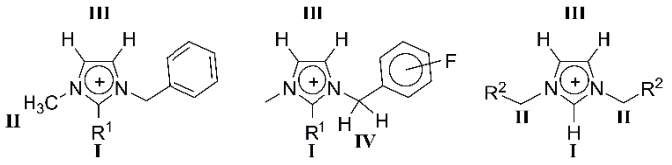

Figure 5. Depiction of four positions (**I–IV**) of the imidazolium cation forming the most pronounced donor-acceptor contacts to the perrhenate anion (left: compounds **1–4**; middle: **5–8**; right: **9–11**).

As the hydrogen atoms are not refined, the donor-acceptor interaction between anion and cation is more accurately reflected by the comparison of the shortest O–C interaction (Table 2). The shortest OH contact of **1** and **2** is formed via the protons located at position I (Figure 5). The methyl protons at the C2 position in **2** are less acidic than the proton in **1**. Further, methylation of the C2 position causes an increased distribution of charge density, resulting in a decrease of the anion-cation interaction (Figure 2). This matches with the elongation of the O–H (and O–C) distance in **2**, being 2.373 Å (3.174(4) Å) when compared to **1** with 2.249 Å (3.027(4) Å) (Table 2, Entries 1 and 2). This corroborates the results obtained from NMR spectroscopy in solution (*vide supra*). The molecular structure of **2** shows that the $[ReO_4]^-$ anion migrates closer to the backbone protons of the cation (Figure 4, right), in contrast to **1**, where the anion is located near the C2 proton (Figure 4, left). However, the introduction of ethyl or isopropyl groups in **3** and **4** does not lead to a change of the O–C interaction (3.079(5) Å (**3**) and 3.141(3) Å (**4**), Figure 6 and SI).

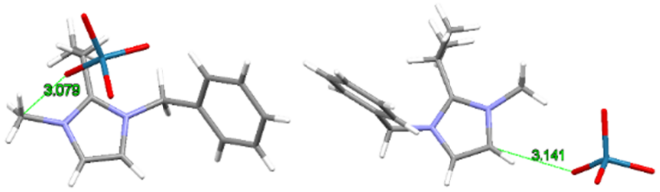

Figure 6. Parts of molecular structures of [MeEtBnIm][ReO_4] (**3**, left) and [Me^{i}PrBnIm][ReO_4] (**4**, right) with the shortest interatomic OC distance (right) (H = white, N = blue, C = grey, Re = turquois, O = red).

This discrepancy from the expected values points out the limitations of X-rays single crystal analysis with regard to the interpretation of donor-acceptor strength from contact distances. Here, packing effects also have to be taken in account, which renders a more detailed discussion difficult, whether the different positions of the $[ReO_4]^-$ anion originate from different proton acidities of the cation, or different steric demands of the ring substituents, i.e. packing effects. On the other hand, very recently it was shown that for imidazolium-based salts in solution, interionic contacts via alkyl protons are as relevant as those with the C2 proton, thus being responsible for the structure of the ionic network.[34]

When a C2 proton is available, this is the desired interaction site of $[ReO_4]^-$ with benzyl-substituted imidazolium salts. Substitution leads to a rearrangement to the methyl group to position I (**2**) and on the nitrogen atom (**3**) (position II).

Table 2. Shortest O–H contacts between $[ReO_4]^-$ and imidazolium and the position of the protons which interact with the anion.[a]

Entry	Compound	Space group	Shortest OH contacts [Å]	Position	Shortest OC contacts [Å]
1	**1**	$P\,2_1\,2_1\,2_1$	2.249	I	3.155 (4)
2	**2**	$P\,1;^-$	2.373	I/CH_3	3.174(4)
3	**3**	$P\,b\,c\,a$	2.368	II	3.079(5)
4	**4**	$P\,2_1/n$	2.255	III	3.141(2)
5	**5**	$P\,2_1/n$	2.220	I	3.110(4)
6	**6**	$C\,2/c$	2.262	IV	3.195(5)
7	**7**	$P\,n\,a\,2_1$	2.286	III	3.214(7)
8	**8**	$P\,2_1\,2_1\,2_1$	2.261	III	3.017(4)
9	**9**	$P\,1;^-$	2.399	I	3.066(5)
10	**10**	$P\,2_1/n$	2.372	II	3.273(3)
11	**11**	$P\,2_1\,2_1\,2_1$	2.264	I	2.989(3)

This is the favoured position, while in the case of the sterically demanding isopropyl group the closest anion relocates towards the backbone (**4**), which leads to a decrease of the O–C interaction (3.141(2) Å).

The compound 1-methyl-3-(2',3',4',5',6'-pentafluorobenzyl)-imidazolium perrhenate (**5**) is a fluorinated analogue of compound **1**. Accordingly, in **5** the perrhenate anion is also located in close contact to the acidic C2 proton with a distance of 3.110(4) Å (see Table 2, Entry 5, Figure 7 and the SI). Unlike the case of compound **2**, methylation of compound **5** results in the migration of the closest perrhenate anion to the proton of the methylene bridge of the Bn^F group (see Figure 7 and SI). This is a result of an increased Lewis acidity of the benzyl methylene protons owing to fluorination of the phenyl ring. This is in agreement with literature reports on the introduction of a Bn^F group on the imidazolium moiety, resulting in stronger OH-interactions.[35,36]

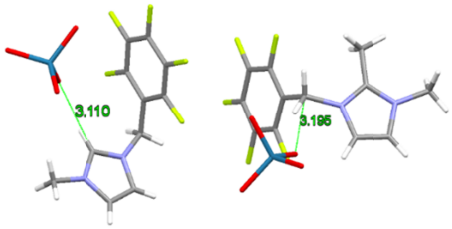

Figure 7. View of the molecular solid-state structure of [MeBn^{F}Im][ReO_4] (**5**) and [MeMeBn^{F}Im][ReO_4] (**6**) with the shortest interatomic OC distance (H = white, N = blue, C = grey, Re = turquois, O = red, F = yellow).

In contrast to compounds **1** and **2**, the insertion of a methyl group at the C2 position of compound **5** does not lead to a contact of perrhenate to the C2 methyl group. The electron-withdrawing character of the Bn^F group increases the acidity of the methylene protons significantly, rendering them more attractive to perrhenate, as seen in the X-ray single crystal structure of compound **6** by a short contact between C2 and O (Figure 7). This increased acidity correlates with a downfield shift in the ^{1}H NMR spectrum of the methylene protons in compound **2** (5.32 ppm) compared to its fluorinated counterpart **6** (5.49 ppm). The Bn^F group apparently provides additional short OH contacts to the perrhenate anion via the methylene bridge (CH_3–$OReO_3$ in compound **2** vs. F_5C_6–CH_2–$OReO_3$ in compound **6**). In compound **5** the anion is also located above

the imidazolium ring and the Bn^F moiety, which is displayed by the high value of OC interactions (Table 3, Entry 5 and Figure 7). This is in contrast to the benzyl-substituted compound **1**. Although this can also be a mere consequence of the ion packing in the unit cell, the effect of the introduction of electron-withdrawing substituents is also visible both in the DFT calculations of the charge distribution and in the NMR shifts, and in the melting points. The Bn^F moiety is also able to provide OF interactions, leading to this relocation. The interaction is visible by the decreased OC interactions and increased OF interactions in **6** (Table 2, Entry 6 and Table 3, Entry 6). This can also be attributed to the acidic protons of the CH_2-C_6F_5 moiety. In the case of sterically more encumbering substituents in the C2 position of Bn^F-substituted imidazolium perrhenates **7** and **8** the anion is forced to move away from the methylene group towards the backbone protons (position **IV**), since the methylene bridge is sterically not accessible, which is a similar effect as in compounds **1** and **4**.

Table 3. Hirshfeld surface analysis of compounds **1**–**11**.[a]

Entry	Compound	OH int. [%][b]	OC int. [%][b]	OF int. [%][b]
1	**1**	85.6	7.4	-
2	**2**	94.2	1.3	-
3	**3**	93.2	1.9	-
4	**4**	89.8	4.0	-
5	**5**	51.3	21.5	16.5
6	**6**	59.8	16.7	18.7
7	**7**	61.1	21.1	12.2
8	**8**	69.1	10.8	16.6
9	**9**	83.4	9.4	-
10	**10**	74.5	6.0	16.6
11	**11**	47.8	23.2	20.7

[a] For details and Hirshfeld surface analysis including fingerprint plots see the SI.

[b] Percentage of the interactions between the oxygen atoms of $[ReO_4]^-$ and hydrogen (OH), carbon (OC) and fluorine atoms (OF) of the imidazolium cation.

This is shown by the crystal structures of compounds **7** and **8** (see SI) and also indicated by the downfield shift of the C2-carbon (Table 1, Entries 7 and 8). Fluorination seems to enhance the interactions between the anion and cation, since the OC interactions increase and OF interactions are possible in the compounds **5**–**8**. The increased interaction is also indicated by additional short O–C contacts of the perrhenate anion to the Bn^F moiety resulting in a short distance of 3.071(4) Å in **5** and 3.070(8) Å in **7** which is also reflected in the Hirshfeld surface analysis of the cations (Figure 8).

The influence of fluorination on the strength of the ion pairing can also be seen in the dibenzyl-substituted compounds **9**–**11**. Although the Hirshfeld surface analysis shows a decrease in the OH interactions from **9**–**11** an increasing degree of fluorination of the benzyl groups results in a decrease of the shortest OC distance and therefore a closer contact of cation and anion (Table 2). The loss of OH interactions is compensated by a distinct increase in OF and OC interactions. Again, this influence could also be determined by DFT calculations for the cations of compounds **10** and **11** (see the SI).

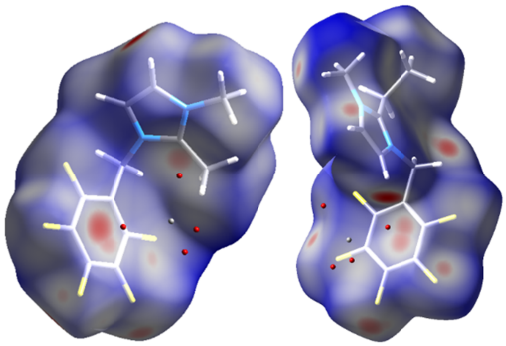

Figure 8. Crystal structure and Hirshfeld surface analysis of $[MeBn^FIm][ReO_4]$ (**5**) and $[MeEtBn^FIm][ReO_4]$ (**7**) with the calculated Hirshfeld surface around the imidazolium cation (blue moiety) to determine deviations of a standard van-der-Waals radius and visualise the interactions between the perrhenate anion and the Bn^F moiety. Red: below standard van-der-Waals radius; Blue: higher than standard van-der-Waals-radius (H = white, N = blue, C = grey, Re = light grey, O = red, F = yellow).

The increase in the OC interactions from **10**–**11** can be explained with the highly symmetric nature of **11** (Figure 9). Compound **10** is an exception as it is the only example where an acidic proton on the C2 position is present but not the shortest contact to the perrhenate anion. A possible reason is again the acidic methylene bridge, which is also visible in ^1H NMR spectroscopy with a downfield shift to from 5.55 ppm (**9**) to 5.68 ppm in **10**. The asymmetric nature of compound **10** is also reflected in the elongated OC contact between anion and cation, which is distinctly larger with 3.273(3) Å compared to 3.006(5) Å in **9** and 2.989(3) Å in **11.** In all other cases with an acidic proton on the C2-position (**1**, **5**, **9** and **11**) the shortest contacts between anion and cation is on that position. This underlines the importance of the acidic C2 position, which seems to act as preferred binding site between cation and anion. However, it seems that in certain cases it is possible to influence the interaction site of anion and cation over the wing tips of the cation.

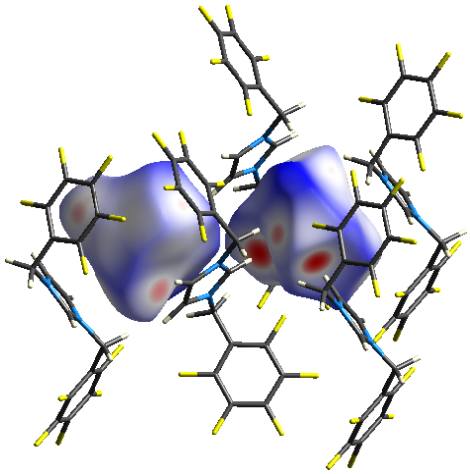

Figure 9. Crystal structure and Hirshfeld surface analysis of compound **11** $[Bn^FBn^FIm][ReO_4]$ with the calculated Hirshfeld surface around the perrhenate anion (blue moiety) to determine deviations of a standard van-der-Waals radius. Red: below standard van-der-Waals radius; Blue: higher than standard van-der-Waals-radius (H = white, N = blue, C = grey, Re = light grey, O = red, F = yellow).

Conclusion

Substitution at the imidazolium ring has an impact on the interaction between the cation and the perrhenate anion. The contacts are based on donor-acceptor interactions, as seen from the molecular structures obtained from X-ray single crystal diffraction. Varying the substitution pattern on the imidazolium ring leads to different ion contacts and hence -strengths, being most pronounced for the alkylation of the C2 position of the ring and for fluorinated N-substituents. The type of interaction largely depends on the substituent at the C2 position between the nitrogen ring atoms, as can be deduced from solution state NMR spectra. Apparently, the acidic Bn^F group allows donor-acceptor contacts, as shown by DFT and X-ray diffraction studies. This is also indicated by a downfield shift of the methylene bridge from **2** to **6** in ^{1}H NMR spectroscopy. Further, Hirshfeld surface analysis shows that fluorination leads to a stronger anion-cation interaction due to a distinct increase of OF and OC contacts, which can also be seen on a macroscopic level. Noteworthy, DFT calculations have shown that the introduction of a second benzyl group on the N atoms has the same effect on the distribution of the positive charge density at the imidazolium ring as alkylation at the C2 position in methyl-benzyl substituted cations.

These results show that at least two effects play a role for the interaction between anion and cation. Alkylation on the C2-position is able to reduce the interactions between anion and cation resulting in an elongation of the shortest donor-acceptor contacts. However, steric demanding substituents force the anion to locate on the backbone protons and reduce these shortest contacts. It has, however, to be noted that this effect can only be qualitatively explained by molecular structures in the solid state, since the changing positions of the anion in dependence of the substituent at the ring can be a consequence of different packing in the unit cell. Nevertheless, indications for the influence of the substituents on the nature and strength of the anion-cation interaction can be found via a combination of solid state analysis methods (single crystal X-ray diffraction, Hirshfeld surface analysis, melting points) together with NMR spectroscopy and DFT studies of the charge density distribution at the cations. With all these methods at hand, at least the origin of the most relevant imidazolium-perrhenate interactions can be localised to a certain extent.

This study of the interionic contacts in imidazolium perrhenates shows that in principle the design of the imidazolium ring has a significant influence on the Coulomb interactions with the perrhenate anion. Considering the reactivity of perrhenate as a nucleophilic agent, a rationalisation of these effects on the ion pairing strength would allow for the synthesis of tailor-made ionic compounds. Further comprehensive studies of a more detailed localisation of the most relevant ion contacts and a quantification of their strengths requires another set of analysis techniques, which is currently underway in our laboratories.

Experimental Section

General remarks. All syntheses were carried out under air, if not stated otherwise. 1,2-Dimethylimidazole was purchased from Acros Organics. 2-Ethylimidazole and 2-isopropyl-imidazole were purchased from Sigma Aldrich. 2,3,4,5,6-Pentafluoro-benzyl bromide and benzyl bromide were purchased from ABCR. All chemicals were used as received without further purification. The imidazolium bromide[35,37-46] and the imidazolium perrhenate salts[29] were synthesised according to literature procedures.

^{1}H-, ^{13}C- and ^{19}F-NMR spectra were recorded on a 400 MHz Bruker Advance DPX-400 spectrometer. ^{1}H- and ^{13}C-NMR spectra were calibrated to the corresponding solvent signals ($CDCl_3$: 7.26 ppm for ^{1}H, 77.16 ppm for ^{13}C; DMSO: 2.50 ppm for ^{1}H, 39.52 ppm for ^{13}C). The ^{19}F-NMR spectra were calibrated by an internal method of the NMR. Microanalysis was performed at the Mikroanalytisches Labor of the Technische Universität München in Garching. The melting points were determined with a MPH-H2 melting point meter from Schorpp Gerätetechnik.

X-ray single crystal diffraction. Data were collected on an X-ray single crystal diffractometer equipped with a CCD detector (APEX II, κ-CCD), a fine focused sealed tube equipped with a graphite monochromator by using the APEXII software package.[47] The measurements were performed on single crystals coated with perfluorinated ether. The crystals were fixed on the top of a glass fiber and transferred to the diffractometer. Crystals were frozen under a stream of cold nitrogen. A matrix scan was used to determine the initial lattice parameters. Reflections were merged and corrected for Lorenz and polarisation effects, scan speed, and background using SAINT.[48] Absorption corrections, including odd and even ordered spherical harmonics were performed using SADABS.[48] Space group assignments were based upon systematic absences, E statistics, and successful refinement of the structures. Structures were solved by direct methods with the aid of successive difference Fourier maps,[49] and were refined against all data using the APEX 2 software in conjunction with SHELXL-2014[49,50] and SHELXLE.[51] Methyl hydrogen atoms were refined as part of rigid rotating groups, with a C–H distance of 0.98 Å and $U_{iso}(H) = 1.5 \cdot U_{eq}(C)$. Other H atoms were placed in calculated positions and refined using a riding model, with methylene and aromatic C–H distances of 0.99 and 0.95 Å, respectively, and $U_{iso}(H) = 1.2 \cdot U_{eq}(C)$. If not mentioned otherwise, non-hydrogen atoms were refined with anisotropic displacement parameters. Full-matrix least-squares refinements were carried out by minimizing $\Sigma w(F_o^2-F_c^2)^2$ with SHELXL-97 weighting scheme.[49,50] Neutral atom scattering factors for all atoms and anomalous dispersion corrections for the non-hydrogen atoms were taken from International Tables for Crystallography.[52] Images of the crystal structures were generated by PLATON.[53] The Hirshfeld surface analysis was carried out with the program Crystal Explorer.[33,54-58] Crystallographic data for the structures of compounds **1**–**11**

have been deposited with the Cambridge Crystallographic Data Centre (**1**: 1030631, **2**: 1030632, **3**: 1030633, **4**: 1030634, **5**: 1030635, **6**: 1030636, **7**: 1030637, **8**: 1030638, **9**: 1030639, **10**: 1030640, **11**: 1030641). Copies of the data can be obtained free of charge from the CCDC, 12 Union Road, Cambridge CB2 1EZ, U.K. (fax +44 1223 336 033; e-mail deposit@ccdc.cam.ac.uk).

Computational details. All calculations have been performed with Gaussian03.[59] The level of theory contains the hybrid DFT functional B3LYP[60,61] and the double zeta 6–31G*[62] basis set for all atoms.

Characterisation data of imidazolium perrhenates

1-Benzyl-3-methylimidazolium perrhenate (**1**): white solid, 85 % yield, m.p.: 71 °C. ^{1}H-NMR (DMSO-d_6, 400 MHz, RT, ppm): δ = 9.17 (s, 1H), 7.76 (s, 1H), 7.69 (s, 1H), 7.41 (m, 5H), 5.40 (s, 2H), 3.85 (s, 3H); ^{13}C-NMR (DMSO-d_6, 100.28 MHz, RT, ppm) δ = 136.7, 134.9, 129.2, 128.4, 124.1, 122.5, 52.1, 36.0; IR (ATR, diamond crystal, neat): v = 899 (Re=O asymmetric); elemental analysis calcd (%) for $C_{11}H_{13}N_2O_4Re$ (423.44): C 31.20, H 3.09, N 6.62, O 15.11, Re 43.97; found: C 31.73, H 3.11, N 6.60, Re 44.03.

1-Benzyl-2,3-dimethylimidazolium perrhenate (**2**): white solid; 76 % yield, m.p.: 112 °C. ^{1}H-NMR ($CDCl_3$, 400 MHz, RT, ppm): δ = 7.43 (m, 3H), 7.28 (d, ^3J = 2.00 Hz, 2H), 7.25 (d, ^3J = 2.00 Hz, 1H), 7.12 (d, ^3J = 2.00, 1H), 5.32 (s, 2H), 3.90 (s, 3H), 2.70 (s, 3H); ^{13}C-NMR (100.28 MHz, DMSO-d_6, RT, ppm) δ = 144.7, 134.7, 129.2, 128.7, 127.8, 122.8, 121.3, 50.7, 35.0, 9.5; IR (ATR, diamond crystal, neat): v = 897 (Re=O asymmetric); elemental analysis calcd. (%) for $C_{12}H_{15}N_2O_4Re$ (437.47): C 32.95, H 3.46, N 6.40, O 14.63, Re 42.56; found: C 33.10, H 3.49, N 6.40, Re 42.75.

1-Benzyl-2-ethyl-3-methylimidazolium perrhenate (**3**): white solid, 90 %, yield m.p.: 91 °C. ^{1}H-NMR ($CDCl_3$, 400 MHz, RT, ppm): δ = 7.42-7.36 (m, 3H), 7.33 (d, ^3J = 2.00 Hz, 1H), 7.27 (m, 1H), 7.25 (m, 1H), 7.21 (d, ^3J = 2.00 Hz, 1H), 5.32 (s, 2H), 3.87 (s, 3H), 3.09 (q, ^3J = 7.60 Hz, 2H), 1.13 (t, ^3J = 8.00, 3H); ^{13}C-NMR (100.28 MHz, $CDCl_3$, RT, ppm) δ = 148.3, 132.9, 129.7, 129.5, 128.1, 123.0, 121.7, 53.8, 52.4, 35.5, 17.3, 10.9; IR (ATR, diamond crystal, neat): v = 897 (Re=O asymmetric); elemental analysis calcd. (%) for $C_{13}H_{17}N_2O_4Re$ (451.49): C 34.58, H 3.79, N 6.20, O 14.17, Re 41.24; found: C 34.60, H 3.69, N 6.10, Re 41.17.

1-Benzyl-2-isopropyl-3-methylimidazolium perrhenate (**4**): white solid, 93 % yield, m.p.: 99 °C. ^{1}H-NMR ($CDCl_3$, 400 MHz, RT, ppm): δ = 7.41-7.33 (m, 4H), 7.23-7.20 (m, 3H), 5.39 (s, 2H), 3.94 (s, 3H), 3.59 (sp, ^3J = 2.00 Hz, 1H), 1.37(d, ^3J = 7.20 Hz, 6H); ^{13}C-NMR (100.28 MHz, $CDCl_3$, RT, ppm) δ = 149.9, 133.2, 129.7, 129.4, 127.7, 124.0, 122.2, 52.7, 36.5, 25.6, 18.7; IR (ATR, diamond crystal, neat): v = 897 (Re=O asymmetric); elemental analysis calcd. (%) for $C_{14}H_{19}N_2O_4Re$ (465.52): C 36.12, H 4.11, N 6.02, O 13.75, Re 40.00; found: C 36.34, H 4.07, N 5.93, Re 39.85.

1-Methyl-3-(2',3',4',5',6'-pentafluorobenzyl)-imidazolium perrhenate (**5**): white solid, 95 % yield, m.p.: 122 °C. ^{1}H-NMR (DMSO-d_6, 400 MHz, RT, ppm): δ = 9.18 (s, 1H), 7.77-7.69 (m, 2H), 5.62 (s, 2H), 3.85 (s, 3H); ^{13}C-NMR (DMSO-d_6, 100.28 MHz, RT, ppm) δ = 137.3, 124.1, 122.7, 36.1; ^{19}F-NMR (DMSO-d_6, 376.46 MHz, RT, ppm) δ =-141.3, -152.9, -161,7; IR (ATR, diamond crystal, neat): v = 895 (Re=O asymmetric); elemental analysis calcd. (%) for $C_{11}H_8F_5N_2O_4Re$ (513.39): C 25.73, H 1.57, F 18.50, N 5.46, O 12.47, Re 36.27; found: C 25.66, H 1.70, F 18.00, N 5.58, Re 36.04.

1,2-Dimethyl-3-(2',3',4',5',6'-pentafluorobenzyl)imidazolium perrhenate (**6**): white solid, 94 % yield, m.p.: 186 °C. ^{1}H-NMR ($CDCl_3$, 400 MHz, RT, ppm): δ = 7.31 (d, ^3J = 2.00 Hz, 1H), 7.28 (d, ^3J = 2.00 Hz, 1H), 5.49 (s, 2H), 3.89 (s, 3H), 2.81 (s, 3H); ^{13}C-NMR (100.28 MHz, DMSO-d_6, RT, ppm) δ = 145.4, 122.8, 122.4, 39.2, 35.0, 9.4; ^{19}F-NMR (376.46 MHz, DMSO-d_6, RT, ppm) δ = -158.7, -149.0, -140.4; IR (ATR, diamond crystal, neat): v = 904 (Re=O asymmetric); elemental analysis calcd. (%) for $C_{12}H_{10}F_5N_2O_4Re$ (527.42): C 27.33, H 1.91, N 5.31, F 18.01, O 12.13, Re 35.31; found: C 27.32, H 1.81, N 5.32, F 18.10, Re 35.62.

2-Ethyl-1-methyl-3-(2',3',4',5',6'-pentafluorobenzyl)imid-azolium perrhenate (**7**): white solid, 96 % yield, m.p.: 119 °C. ^{1}H-NMR (DMSO-d_6, 400 MHz, RT, ppm): δ = 7.69 (d, ^3J = 2.00 Hz, 1H), 7.63 (d, ^3J = 2.00 Hz, 1H), 5.63 (s, 2H), 3.83 (s, 3H), 3.11 (q, ^3J = 7.60 Hz, 2H), 1.16 (t, ^3J = 7.60 Hz, 3H); ^{13}C-NMR (100.28 MHz, DMSO-d_6, RT, ppm) δ = 148.4, 123.2, 121.3, 34.7, 16.2, 10.4; ^{19}F-NMR (376.46 MHz, DMSO-d6, RT, ppm) δ = -161.5, -152.6, -141.3; IR (ATR, diamond crystal, neat): v = 905 (Re=O asymmetric); elemental analysis calcd. (%) for $C_{13}H_{12}F_5N_2O_4Re$ (541.44): C 28.84, H 2.23, N 5.17, F 17.54, O 11.82, Re 34.39; found: C 29.00, H 2.40, N 5.16, F 17.56, Re 34.49.

2-Isopropyl-1-methyl-3-(2',3',4',5',6'-pentafluorobenzyl)-imidazolium perrhenate (**8**): white solid, 90 % yield, m.p.: 164 °C. ^{1}H-NMR (DMSO-d_6, 400 MHz, RT, ppm): δ = 7.68 (d, ^3J = 2.00 Hz, 1H), 7.59 (d, ^3J = 2.00 Hz, 1H), 5.68 (s, 2H), 3.70 (sp, ^3J = 7.20 Hz, 1H), 1.39 (d, ^3J = 7.60 Hz, 6H); ^{13}C-NMR (100.28 MHz, DMSO-d_6, RT, ppm) δ = 149.6, 124.2, 121.3, 36.2, 24.3, 18.0; ^{19}F-NMR (376.46 MHz, DMSO-d_6, RT, ppm) δ = -161.4, -152.6, -141.4; IR (ATR, diamond crystal, neat): v = 904 (Re=O asymmetric); elemental analysis calcd. (%) for $C_{14}H_{14}F_5N_2O_4Re$ (555.47): C 30.27, H 2.54, N 5.04, F 17.10, O 11.52, Re 33.52; found: C 30.39, H 2.62, N 5.02, F 16.90, Re 33.38.

1,3-Dibenzylimidazolium perrhenate (**9**): white solid, 80 % yield, m.p.: 101 °C. ^{1}H-NMR ($CDCl_3$, 400 MHz, RT, ppm): δ = 10.89 (s, 1H), 7.46 (m, 4H), 7.37 (m, 6H), 7.19 (s, 2H), 5.55 (s, 4H); ^{13}C-NMR ($CDCl_3$, 100 MHz, RT, ppm): δ = 137.5, 132.9, 129.8, 129.7, 129.3, 121.9, 53.73; IR (ATR, diamond crystal, neat): v = 904 (Re=O asymmetric);elemental analysis calcd (%) for $C_{17}H_{17}N_2O_4Re$ (499.53): C 40.87, H 3.43, N 5.61, O 12.81, Re 37.28; found: C 41.18, H 3.36, N 5.56, Re 37.28.

1-Benzyl-3-(2',3',4',5',6'-pentafluorobenzyl)imidazolium perrhenate (**10**): white solid, 91 % yield, m.p.: 102 °C. ^{1}H-NMR (DMSO-d_6, 400 MHz, RT, ppm): δ = 9.47 (s, 1H), 7.87 (dd, ^3J = 1.8 Hz, 1H),7.83 (dd, ^3J = 1.8 Hz, 1H), 7.44 (m, 5H), 5.68 (s, 2H), 5.45 (s, 2H); ^{13}C-NMR (DMSO-d_6, 100.28 MHz,

RT, ppm): δ = 136.9, 134.6, 129.0, 128.8, 128.3, 123.1, 122.8, 52.1; ^{19}F-NMR (DMSO-d_6, 376.46 MHz, RT, ppm): δ = -161.23, -152.4, -140.90; IR (ATR, diamond crystal, neat): v = 905 (Re=O asymmetric); elemental analysis calcd. (%) for $C_{17}H_{12}F_5N_2O_4Re$ (589.49): C 34.64, H 2.05, F 16.11, N 4.75, O 10.86, Re 31.59; found: C 34.49, H 2.05, N 4.78, 31.11.

1,3-Di(2',3',4',5',6'-pentafluorobenzyl)imidazolium-perrhenate (**11**): white solid, 92 % yield, m.p.: 176 °C. ^{1}H-NMR (D_2O, 400 MHz, RT, ppm): δ = 9.26 (s, 1H), 7.58 (s, 2H), 5.62 (s, 4H); ^{13}C-NMR (D_2O, 100.28 MHz, RT, ppm): δ = 122.0, 120.4, 40.0; 19F-NMR (DMSO-d_6, 376.46 MHz, RT, ppm): δ = -161.6, -151.9, -142.7; IR (ATR, diamond crystal, neat): v = 904 (Re=O asymmetric); elemental analysis calcd. (%) for $C_{17}H_7F_{10}N_2O_4Re$ (679.44): C 30.05, H 1.04, F 27.96, N 4.12, O 9.42, Re 27.41; found: C 30.20, H 0.92, F 28.01, N 3.97, Re 27.34.

Acknowledgements

R.M.R., I.I.E.M. and C.J.M. thank the TUM Graduate School for financial support. The authors further thank Dr. M. H. Anthofer, M. E. Wilhelm and Dr. M. Drees for their support and valuable discussions.

Notes and references

Chair of Inorganic Chemistry/Molecular Catalysis, Department of Chemistry and Catalysis Research Center, Technische Universität München, Lichtenbergstraße 4, D-85747 Garching bei München (Germany). E-mails: mirza.cokoja@tum.de, fritz.kuehn@ch.tum.de

Supplementary Information (SI) available: X-ray crystallography data, details of the Hirshfeld surface analysis and computational details. See DOI: 10.1039/b000000x/

1. M. J. Earle and K. R. Seddon, *Pure Appl. Chem.*, 2000, **72**, 1391–1398.
2. C. Münchmeyer, L. Graser, I. E. Markovits, M. Cokoja and F. Kühn, *Top. Organomet. Chem.* DOI: 10.1007/3418_2013_66.
3. Y. Ito and T. Nohira, *Electrochim. Acta*, 2000, **45**, 2611–2622.
4. T. Welton, *Chem Rev*, 1999, **99**, 2071–2084.
5. L. A. Blanchard, D. Hancu, E. J. Beckman and J. F. Brennecke, *Nature*, 1999, **399**, 28–29.
6. A. Fernandez, J. S. Torrecilla, J. Garcia and F. Rodriguez, *J. Chem. Eng. Data*, 2007, **52**, 1979–1983.
7. P. Wasserscheid, *Nature*, 2006, **439**, 797–797.
8. F. Endres and S. Z. El Abedin, *Phys. Chem. Chem. Phys.*, 2006, **8**, 2101–2116.
9. M. E. van Valkenburg, R. L. Vaughn, M. Williams and J. S. Wilkes, *Thermochim. Acta*, 2005, **425**, 181–188.
10. R. Hagiwara, Y. Nakamori, K. Matsumoto and Y. Ito, *J. Phys. Chem. B*, 2005, **109**, 5445–5449.
11. R. D. Rogers and K. R. Seddon, *Science*, 2003, **302**, 792–793.
12. K. Noack, P. S. Schulz, N. Paape, J. Kiefer, P. Wasserscheid and A. Leipertz, *Phys Chem Chem Phys*, 2010, **12**, 14153–14161.
13. J. M. Slattery, C. Daguenet, P. J. Dyson, T. J. S. Schubert and I. Krossing, *Angew. Chem. Int. Ed.*, 2007, **46**, 5384–5388.
14. S. A. Katsyuba, E. E. Zvereva, A. Vidis and P. J. Dyson, *J. Phys. Chem. A*, 2007, **111**, 352–370.
15. E. A. Turner, C. C. Pye and R. D. Singer, *J. Phys. Chem. A*, 2003, **107**, 2277–2288.
16. J. Kiefer and C. C. Pye, *J. Phys. Chem. A*, 2010, **114**, 6713–6720.
17. N. R. Dhumal, H. J. Kim and J. Kiefer, *J. Phys. Chem. A*, 2009, **113**, 10397–10404.
18. J. C. Lassègues, J. Grondin, R. Holomb and P. Johansson, *J. Raman Spectrosc.*, 2007, **38**, 551–558.
19. J. Kiefer, J. Fries and A. Leipertz, *Appl. Spectrosc.*, 2007, **61**, 1306–1311.
20. P. A. Hunt, B. Kirchner and T. Welton, *Chem. Eur. J.*, 2006, **12**, 6762–6775.
21. Y. Chauvin, L. Mussmann and H. Olivier, *Angew. Chem. Int. Ed. Engl.*, 1996, **34**, 2698–2700.
22. K. Fumino, A. Wulf and R. Ludwig, *Angew. Chem. Int. Ed.*, 2008, **47**, 8731–8734.
23. P. A. Hunt, I. R. Gould and B. Kirchner, *Aust. J. Chem.*, 2007, **60**, 9–14.
24. P. A. Hunt, *J. Phys. Chem. B*, 2007, **111**, 4844–4853.
25. S. A. Katsyuba, P. J. Dyson, E. E. Vandyukova, A. V. Chernova and A. Vidiš, *Helv. Chim. Acta*, 2004, **87**, 2556–2565.
26. S. Stolte, T. Schulz, C.-W. Cho, J. Arning and T. Strassner, *ACS Sustainable Chem. Eng.*, 2013, **1**, 410–418.
27. S. Ahrens, A. Peritz and T. Strassner, *Angew. Chem. Int. Ed.* **2009**, *48*, 7908–7910.
28. D.-W. Fang, H. Wang, S. Yue, Y. Xiong, J.-Z. Yang and S.-L. Zang, *J. Phys. Chem. B*, 2012, **116**, 2513–2519.
29. I. I. E. Markovits, W. A. Eger, S. Yue, M. Cokoja, C. J. M. Münchmeyer, B. Zhang, M. D. Zhou, A. Genest, J. Mink, S. L. Zang, N. Rösch and F. E. Kühn, *Chem. Eur. J.*, 2013, **19**, 5972–5979.
30. C. A. Angell, N. Byrne and J.-P. Belieres, *Acc. Chem. Res.*, 2007, **40**, 1228–1236.
31. R. J. C. Brown and R. F. C. Brown, *J. Chem. Educ.*, 2000, **77**, 724–731.
32. G. Gurau, H. Rodríguez, S. P. Kelley, P. Janiczek, R. S. Kalb and R. D. Rogers, *Angew. Chem. Int. Ed.*, 2011, **50**, 12024–12026.
33. M. A. Spackman and D. Jayatilaka, *CrystEngComm*, 2009, **11**, 19–32.
34. A. Khrizman, H. Y. Cheng, G. Bottini and G. Moyna, *Chem. Commun.*, 2015, **51**, 3193–3195.
35. M. E. Wilhelm, M. H. Anthofer, R. M. Reich, V. D'Elia, J.-M. Basset, W. A. Herrmann, M. Cokoja and F. E. Kühn, *Catal. Sci. Technol.*, 2014, **4**, 1638–1643.
36. J. M. Serrano-Becerra, S. Hernandez-Ortega, D. Morales-Morales and J. Valdes-Martinez, *CrystEngComm*, 2009, **11**, 226–228.
37. M. H. Anthofer, M. E. Wilhelm, M. Cokoja, I. I. E. Markovits, A. Pothig, J. Mink, W. A. Herrmann and F. E. Kuhn, *Catal. Sci. Technol.*, 2014, **4**, 1749–1758.
38. N. Kumar and R. Jain, *J. Heterocyclic Chem.*, 2012, **49**, 370–374.
39. J. R. Harjani, J. Farrell, M. T. Garcia, R. D. Singer and P. J. Scammells, *Green Chem.*, 2009, **11**, 821–829.
40. E. Ennis and S. Handy, *Molecules*, 2009, **14**, 2235–2245.
41. C. Betti, D. Landini and A. Maia, *Tetrahedron*, 2008, **64**, 1689–1695.
42. S. T. Handy, *J. Org. Chem.*, 2006, **71**, 4659–4662.

43. M. Debdab, F. Mongin and J. P. Bazureau, *Synthesis*, 2006, **23**, 4046–4052.
44. S. McGrandle and G. C. Saunders, *J. Fluorine Chem.*, 2005, **126**, 449–453.
45. N. L. Lancaster, P. A. Salter, T. Welton and G. B. Young, *J. Org. Chem.*, 2002, **67**, 8855–8861.
46. R. E. Wasylishen, G. S. Birdi and A. F. Janzen, *Inorg. Chem.*, 1976, **15**, 3054–3056.
47. APEX suite of crystallographic software. APEX 2 Version, Madison, Wisconsin, USA, 2008.
48. SAINT, Version 7.56a and SADABS Version 2008/1., Madison, Wisconsin, USA, 2008.
49. G. M. Sheldrick, SHELXS-97, Program for Crystal Structure Solution, Göttingen, 1997.
50. G. M. Sheldrick, SHELXL-2014, University of Göttingen, Germany, 2014.
51. C. B. Hübschle, G. M. Sheldrick and B. Dittrich, *J. Appl. Crystallogr.*, 2011, **44**, 1281–1284.
52. A. J. C. Wilson, International Tables for Crystallography, Dordrecht, The Netherlands Tables 6.1.1.4 (pp. 500-502), 4.2.6.8 (pp. 219-222), and 4.2.4.2 (pp. 193-199)*, Kluwer Academic Publishers* 1992, *Vol. C*.
53. A. L. Spek, PLATON, A Multipurpose Crystallographic Tool, Utrecht University, Utrecht, The Netherlands, 2010.
54. M. J. Turner, J. J. McKinnon, D. Jayatilaka and M. A. Spackman, *CrystEngComm*, 2011, **13**, 1804-1813.
55. M. A. Spackman, J. J. McKinnon and D. Jayatilaka, *CrystEngComm*, 2008, **10**, 377-388.
56. J. J. McKinnon, D. Jayatilaka and M. A. Spackman, *Chem. Commun.*, 2007, 3814-3816.
57. J. J. McKinnon, M. A. Spackman and A. S. Mitchell, *Acta Crystallogr., Sect. B: Struct. Sci.*, 2004, **60**, 627-668.
58. M. A. Spackman and J. J. McKinnon, *CrystEngComm*, 2002, **4**, 378-392.
59. M. J. Frisch et al., Gaussian03, Gaussian, Inc., Wallingford, CT, 2004.
60. A. D. Becke, *J. Chem. Phys.*, 1993, **98**, 5648–5652.
61. Y. W. C. Lee and R. G. Parr, *Phys. Rev. B: Condens. Matter.* 1988, **37**, 785–789.
62. W. J. Hehre, R. Ditchfield and J. A. Pople, *J. Chem. Phys.*, 1972, **56**, 2257–2261.